Journal of Materials Chemistry A

ROYAL SOCIETY OF CHEMISTRY

PAPER

View Article Online
View Journal | View Issue

Cite this: J. Mater. Chem. A, 2022, 10, 22812

A *meta*-alkylthio-phenyl chain–substituted small-molecule donor as the third component for high-efficiency organic solar cells†

Chenyang Zhang,[a] Jing Li,[a] Lei Ji,[a] Hanlin Hu,*[b] Gang Li*[c] and Kai Wang*[a]

Ternary organic solar cells (OSCs) have attracted increasing attention because they are a feasible and efficient strategy to improve the power conversion efficiency (PCE) of OSCs. However, the rational molecular design of guest materials with a suitable absorption spectrum, energy level and molecular packing is still challenging. Herein, a large-bandgap small-molecule (SM) donor, BTC, incorporated with *meta*-alkylthio-phenyl-substituted benzo[1,2-*b* : 4,5-*b*′]dithiophene (BDT) as the core, was designed and synthesized for high-performance ternary OSCs. It possesses a deeper HOMO (highest occupied molecular orbital) level compared to PM6, which leads to a higher open-circuit voltage (V_{OC}). Moreover, BTC exhibits good miscibility and complementary absorption with PM6 in the near-ultraviolet region, favoring the photovoltaic performance of OSCs by enhancing the short-circuit current density (J_{SC}). Additionally, the ternary blend film with 15 wt% BTC achieved an optimized morphology with a nanofibrous network and strong face-on molecular stack, resulting in higher and more balanced charge mobilities, lower charge recombination and more efficient exciton dissociation compared to the binary blend. Therefore, we have successfully demonstrated a PCE of 17.32% for the ternary OSCs with 15 wt% BTC, with simultaneously improved V_{OC}, J_{SC} and FF compared to the PM6 : Y6 binary OSCs (15.51%). Moreover, the replacement of the acceptor with L8-BO further improves the PCE of ternary OSCs by up to 18.41%. This study provides a promising building block and effective design to fulfill the prerequisites of the absorption spectrum, molecular packing, energetics, and miscibility of small-molecule donors to achieve high-performance ternary OSCs.

Received 24th August 2022
Accepted 2nd October 2022

DOI: 10.1039/d2ta06706d

rsc.li/materials-a

Introduction

Bulk heterojunction (BHJ) OSCs have attracted tremendous attention due to their various advantages, such as mechanical flexibility, solution-processed capacity, light weight, and semi-transparency.[1–6] In recent years, OSCs have undergone rapid progress due to the emergence of non-fullerene acceptors, *e.g.*, ITIC,[7] IT-4F,[8] O-IDTBR,[9] PTIC,[10] and Y6.[11,12] Single-junction binary OSCs with Y6 and its derivatives as acceptors afford high PCEs of over 17%.[13–15] To further improve device efficiency, the concept of ternary OSCs, where the active layers comprise either two donors with one acceptor or one donor with two acceptors, has been extensively explored.[16–24] Compared with binary OSCs, ternary OSCs have several advantages: (i) a suitable third component may cause cascade energetics alignment with the binary host, thereby facilitating charge transfer and promoting the V_{OC};[24–28] (ii) the third component can broaden the absorption and increase the J_{SC};[29] (iii) it can tailor the morphology and crystallinity of the active layer to increase exciton dissociation and charge transfer ability. Owing to these benefits, many efforts have been devoted to develop ternary OSCs, and great progress has been achieved through the rational selection of the third component.[30–34] Besides the BHJ structure, Zhang *et al.* reported that the ternary strategy shows a significant improvement in the performance of OSCs *via* a layer-by-layer (LbL) structure.[35]

Recently, PM6 : Y6-based OSCs have been recognized as a representative high-efficiency binary system and are widely adopted as the host of ternary OSCs because the trade-off between the three photovoltaic parameters is already low. It has been demonstrated that introducing another acceptor (fullerene derivatives[36–40] or non-fullerene acceptors[36,41,42]) as the second acceptor can enhance the device performance due to the complementary absorption spectra and efficient energy level cascade. For example, Chen *et al.* adopted the BTP-M acceptor into PM6 : Y6 to construct ternary OSCs. The compatible and similar chemical structures of BTP-M and Y6 resulted in the

[a]Institute of Flexible Electronics (IFE), Northwestern Polytechnical University (NPU), Xi'an 710072, China. E-mail: kaiwang@nwpu.edu.cn

[b]Hoffman Institute of Advanced Materials, Shenzhen Polytechnic, 7098 Liuxian Boulevard, Shenzhen 518055, China. E-mail: hanlinhu@szpt.edu.cn

[c]Department of Electronic and Information Engineering, Research Institute for Smart Energy (RISE), The Hong Kong Polytechnic University, Hung Hom, Kowloon, Hong Kong, China. E-mail: gang.w.li@polyu.edu.hk

† Electronic supplementary information (ESI) available. See DOI: https://doi.org/10.1039/d2ta06706d

formation of alloy-like models.[20] A high PCE of 17.03% was obtained with suppressed energy loss and an optimized morphology of the active layer. Zhan *et al.* incorporated the non-fullerene acceptor IN-4F as the third acceptor into a PM6 : Y6 binary blend. The resultant ternary OSCs delivered enhanced V_{OC} and J_{SC} owing to the higher LUMO (lowest unoccupied molecular orbital) and increased charge mobilities.[43]

However, reports on efficient ternary OSCs based on PM6 : Y6 using SM as the third component are relatively rare so far. A crucial challenge is balancing the contradiction between the absorption and energy levels of the donor. In contrast to polymers, SM donors have the intrinsic advantages of an easier purification method, a definite chemical structure, and less batch variation, thus showing great promise in constructing ternary OSCs. Zhang *et al.* reported that good compatibility of the third component with the host can provide an opportunity to finely optimize the morphology of the active layers, and thus favor the device performance.[44] Ge *et al.* introduced the SM donor SM1 into the PM6 : Y6 binary blend and constructed ternary OSCs. A high PCE of 16.55% was obtained with improved charge extraction and exciton dissociation.[45] Li *et al.* developed the SM donor BPR-SCl to fabricate ternary OSCs. The incorporation of BPR-SCl enhanced the exciton dissociation, charge mobilities and molecular packing, yielding a high PCE of 16.74%.[46] Tan *et al.* developed a large-bandgap SM donor (BTBR-2F) based on intramolecular noncovalent C–H···F interaction to achieve a coplanar structure and tight intermolecular packing. Benefiting from the complementary absorption with the PM6 : Y6 system, more efficient exciton dissociation and higher mobilities, the resultant devices achieved a high PCE of 17.38%.[47] Several ternary OSCs based on the PM6 : Y6 binary blend with small-molecule donors as guests have been developed. However, as shown in Table S1,† a PCE of over 17% is still rare, and it is of great interest and necessity to explore novel small-molecule donors for efficient ternary OSCs.

Substituting the thiophene side groups with phenyl units in the BDT unit has proven to be an effective strategy for tuning the molecular orientation and improving device performance. Hou *et al.* reported the SM donor B1 with phenyl-substituted BDT as the core. The resultant device outperformed the thiophene side group-substituted donor-based devices due to its enhanced exciton dissociation and improved morphology.[48] In view of the above, a novel SM donor, BTC (Fig. 1a), incorporating *meta*-alkylthio-phenyl-substituted BDT as the core, octyl-substituted terthiophene as the π-conjugated bridge and octyl-2-cyanoacrylate as the terminal group, was designed and synthesized to construct efficient ternary OSCs. BTC exhibits a complementary absorption with the PM6 : Y6 binary blend, thereby enhancing photo harvesting. Superior miscibility and well-mixed phases were observed between BTC and PM6. Furthermore, the improved morphology and crystallinity mediation lead to enhanced and balanced charge transport ability with reduced charge recombination in the ternary OSCs. Therefore, the ternary OSCs with 15 wt% BTC exhibited a PCE of 17.32% with synchronously improved V_{OC} (0.834 V), J_{SC} (28.00 mA cm^{-2}) and FF (73.51%) compared with the PM6 : Y6 devices. Furthermore, to test the universality of BTC, ternary OSCs based on the PM6 : L8-BO system were also studied. A PCE enhancement from 17.62% to 18.41% was obtained when incorporating 15 wt% BTC. To the best of our knowledge, this may be one of the highest PCEs in ternary OCSs with an SM donor. Overall, this work demonstrates that introducing the alkylthio-phenyl chain group is an effective strategy to develop small-molecule donors to finely tune the absorption spectra, molecular packing and energy levels for high-performance ternary OSCs.

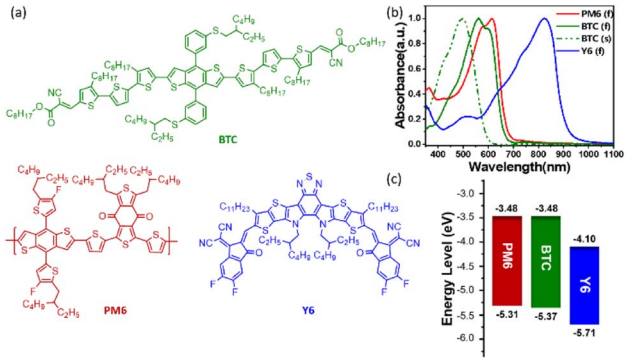

Fig. 1 (a) Structures of BTC, PM6 and Y6, (b) normalized absorption of the PM6, BTC and Y6 films and BTC in chloroform solution, and (c) energy levels of PM6, BTC and Y6.

Results and discussion

Synthesis and properties

Fig. 1a outlines the chemical structures of the SM donor (5*Z*,5′*Z*)-5,5′-(((4,8-bis(3-((2-ethylhexyl)thio)phenyl)benzo[1,2-*b* : 4,5-*b*′]dithiophene-2,6-diyl)-bis(3,3″-dioctyl-[2,2′ : 5′,2″-terthiophene]-5″,5-diyl))(2*E*,2′*E*)-bis(octyl-2-cyanoacrylate)) (BTC), PM6 and Y6. Further synthetic details and structural confirmation, including the ^{1}H NMR, ^{13}C NMR, and mass spectra, are provided in the (ESI†). Pd-mediated Stille cross-coupling afforded the target molecule with a yield of 60%. The molecule is soluble in common solvents. The thermogravimetric analyses (TGA) shown in Fig. S4† indicate that BTC is thermally stable in a nitrogen atmosphere until *ca.* 352 °C (*ca.* 5% weight loss). Fig. 1b presents the normalized absorption spectra of BTC. The PM6 and Y6 films exhibit extensive absorption in the ranges of 500–650 and 640–900 nm, respectively, whereas the absorption of BTC shows a blue shift of 54 nm for the maximum peak compared with PM6. The optical bandgap of BTC (1.89 eV) is larger than that of PM6 (1.83 eV). Therefore, it directly indicates complementary absorption in the range of 450–600 nm, which is beneficial for light harvesting in the short-wavelength region. Density functional theory (DFT) calculation shows that the HOMO is mainly localized at the BDT core and terthiophene bridge, while the LUMO situates on the cyanoacrylate unit and thiophene unit.[49] The calculated HOMO and LUMO levels are −5.33 and −3.12 eV, respectively (Fig. S5†). The *meta*-alkylthio-phenyl chain shows a torsion angle of 60.3° with the BDT backbone. All adjacent thiophene units in the BTC backbone show small dihedral angles (<10°), indicating the good planarity of the molecular backbone, which favors close intermolecular

π–π stacking and charge transfer (Fig. S6†). Cyclic voltammetry (CV) was carried out to estimate the energy levels of BTC and PM6, and the results are depicted in Fig. S7.† Both of them show the same LUMO level of −3.48 eV, and the HOMO levels are calculated to be −5.31 and −5.37 eV for PM6 and BTC, respectively, inferred from the LUMO and optical bandgap (E_g). The lower lying HOMO of BTC compared to that of PM6 could provide a cascade for hole transfer, benefitting the V_{OC} and J_{SC} compared to those of binary OSCs (Fig. 1c).

Device performance

The photovoltaic properties of the binary and ternary OSCs were examined with an inverted structure of ITO/ZnO/active layer/MoO_3/Ag. All devices were produced by spin-coating a chloroform solution supplemented with 0.5 vol% 1-chloronaphthalene and the total concentration of the host was kept at 16 mg mL^{-1}. The binary OSCs had different donor/acceptor weight ratios, with PM6 : Y6 at 1 : 1.2 and BTC : Y6 at 2 : 1, and that of the ternary OSCs was 1 : 0.15 : 1.2. All the devices were tested under standard AM 1.5 G illumination with 100 mW cm^{-2} intensity in air. The current density–voltage (J–V) curves and photovoltaic parameters are summarized in Fig. 2 and Table 1. The devices were mainly optimized by adjusting the guest : donor ratios and the annealing temperature. Detailed optimization information is provided in Table S2–S6 and Fig. S8.† The binary OSCs (PM6 : Y6) exhibited a PCE of 15.51%, V_{OC} of 0.826 V, J_{SC} of 26.21 mA cm^{-2} and FF of 71.63%, in line with the reported values in the literature.[11] The BTC : Y6 binary OSCs showed a lower PCE of 7.48% at an optimal ratio of 2 : 1 under annealing conditions at 120 °C for 15 min. We then fabricated ternary OSCs with BTC as the second donor. When the BTC weight ratio in the ternary OSCs increases, the V_{OC} values gradually increase from 0.828 to 0.839 V. Thus, considering the good miscibility between PM6 and BTC, an "alloy-like" state should be formed.[50] The HOMO energy level of the "alloy-like" donor may be slightly adjusted by altering the BTC ratio, resulting in the gradually increasing V_{OC} of the ternary OSCs.[51] The BTC : Y6 binary OSCs showed a low V_{OC} of 0.801 V. This might be ascribed to the severe exciton recombination and weak charge transport due to the inferior morphology.[52] The J_{SC} value of the binary control PM6 : Y6 OSCs is 26.21 mA cm^{-2}, which increased to 28.00 mA cm^{-2} after the introduction of 15 wt% BTC. The BTC film shows a slightly lower absorption coefficient than the PM6 film. The blend film of PM6 : 15 wt% BTC exhibits a higher absorption coefficient than those of the neat PM6 and BTC films (Fig. S9†), which improves the light-harvesting capability. Therefore, the improvement in J_{SC} could be attributed to the enhanced absorption of BTC in the short-wavelength region and the possibly optimized morphology of the ternary blend layer. As shown in the external quantum efficiency (EQE) spectra (Fig. 2c), compared to the PM6 : Y6 device, the ternary OSCs incorporating 15 wt% BTC exhibit an increased photoresponse in the 400–500 nm region. The integrated photocurrents (J_{SC}^{cal}) from the EQE spectra of PM6 : Y6, PM6 : BTC : Y6 and BTC : Y6 are 25.74, 27.16 and 17.88 mA cm^{-2}, respectively (Table 1), in agreement with the J_{SC} values in the J–V curves within 5% error. Compared to the PM6 : Y6 binary system, the FF of the ternary OSCs increased from 70.9% to 73.3%. The series resistance (R_S) and shunt resistance (R_{SH}) of the binary and ternary OSCs extracted from their J–V curves are presented in Table 1. It is obvious that the slightly reduced R_S and enhanced R_{SH} values of the optimal ternary OSCs compared to those of the binary OSCs contribute to the increased FF in the ternary OSCs.[53] Ultimately, the ternary OSCs of PM6:15 wt% BTC : Y6 delivered a remarkable PCE of 17.3% with simultaneously improved V_{OC}, J_{SC} and FF, considerably higher than the 15.51% (PM6 : Y6) and 7.48% (BTC : Y6) of the binary OSCs.

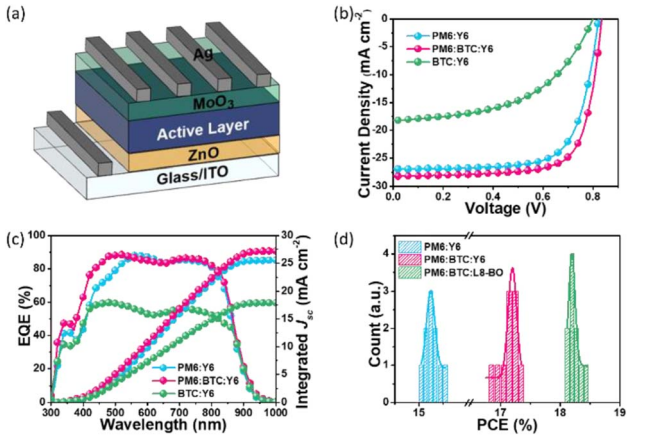

Fig. 2 (a) A schematic of the device architecture, (b) current density–voltage (J–V) curves, (c) EQE spectra, and (d) statistics of PCE values for the binary and ternary OSCs.

Morphological characterization

To understand the miscibility between PM6 : Y6 and BTC, the Flory–Huggins interaction parameters (χ) were calculated using

Table 1 Summary of the device performance of the binary and optimized ternary OSCs

Active layer	V_{OC} [V]	J_{SC} [mA cm^{-2}]	J_{SC}^{cal} [mA cm^{-2}]	FF [%]	PCE_{ave}[a] (PCE_{max}) [%]	R_S [Ω cm^2]	R_{SH} [Ω cm^2]
PM6 : Y6	0.824 ± 0.002	26.14 ± 0.16	25.74	70.94 ± 0.50	15.27 ± 0.13 (15.51)	4.33	873
PM6 : BTC : Y6	0.834 ± 0.006	28.00 ± 0.27	27.16	73.35 ± 0.44	17.13 ± 0.16 (17.32)	4.18	1772
BTC : Y6	0.795 ± 0.003	18.25 ± 0.05	17.88	49.74 ± 0.83	7.20 ± 0.15 (7.48)	12.31	305
PM6 : L8-BO	0.887 ± 0.001	26.18 ± 0.03	25.10	75.59 ± 0.26	17.55 ± 0.10 (17.62)	4.35	1003
PM6 : BTC : L8-BO	0.895 ± 0.001	26.74 ± 0.09	25.63	76.23 ± 0.19	18.24 ± 0.09 (18.41)	4.03	1910

[a] Average values are based on 10 devices from different batches.

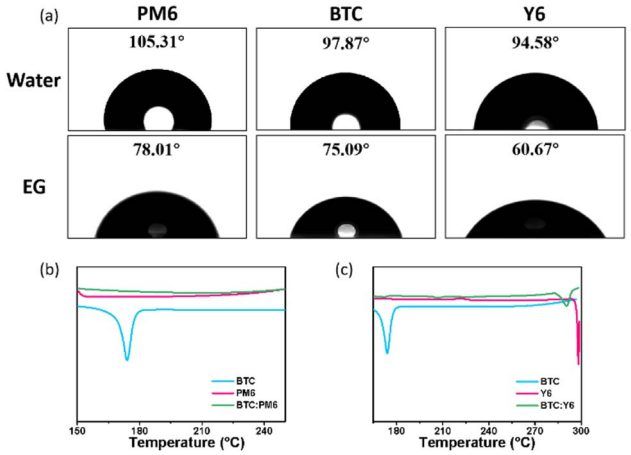

Fig. 3 (a) Contact angle images of the PM6, BTC, and Y6 films. DSC curves of (b) PM6, BTC, and PM6 : BTC (20 : 3 by weight) and (c) BTC, Y6, and Y6 : BTC (8 : 1 by weight).

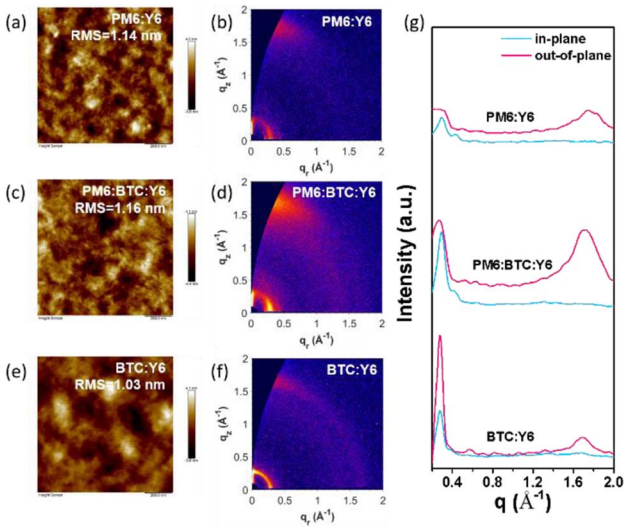

Fig. 4 AFM height and GIWAXS images of PM6 : Y6 (a and b), PM6 : BTC : Y6 (1 : 0.15 : 1.2) (c and d), and BTC : Y6 (e and f); (g) scattering profiles of the corresponding films.

$\chi_{A:D} = K(\sqrt{\gamma_A} - \sqrt{\gamma_D})^2$.[54] The contact angles and calculated results are shown in Fig. 3a. The surface energies of PM6, BTC and Y6 are calculated to be 25.08 mN m^{-1}, 21.27 mN m^{-1} and 37.03 mN m^{-1}, respectively, using the Owens–Wendt–Kaelble equation. Next, the Flory–Huggins interaction parameter between the two materials was estimated based on the surface energy.[47] The χ value between BTC and PM6 is 0.16 K, while that between BTC and Y6 is 2.17 K (Table 2). A smaller χ value generally represents better miscibility.[54] Therefore, BTC would rather disperse in the PM6 phase than in the Y6 phase in the ternary blend. To further investigate the miscibility of BTC, differential scanning calorimetry (DSC) was utilized. As shown in Fig. 3b and S10,† BTC exhibits a melting peak of 174 °C, whereas PM6 does not show melting and crystallization peaks within the tested temperature range. The melting peak disappeared when blended with PM6 (PM6 : BTC, w/w = 20 : 3), which indicates that BTC should be completely miscible with PM6. However, Y6 shows a melting point at *ca.* 298 °C, and the melting temperature decreases to 290.5 °C in the Y6 and BTC mixture (Y6 : BTC, w/w = 8 : 1) with a broad peak. An endothermic peak at 174 °C exists in the Y6 and BTC mixture, which should be the melting peak of BTC, indicating that BTC and Y6 are less compatible in the blend. As a result, BTC is mainly distributed in the PM6 domain with a minor amount dispersed in Y6, which is consistent with the contact angle measurements.[20]

The thin-film topography was tested using atomic force microscopy (AFM). Fig. 4a presents a smooth surface with a root mean square (RMS) roughness of 1.14 nm for the PM6 : Y6 blend. With the introduction of 15 wt% BTC, the surface morphology does not change significantly, as evidenced by the relatively smoother surface with an RMS of 1.16 nm (Fig. 4c), which indicates that both films have good interfacial contact with the upper electrode.[35] Meanwhile, both the binary and ternary films exhibit a phase image of a bicontinuous nanofibrous network structure (Fig. S11a and b†). However, the BTC : Y6 film shows a sea-island phase separation and large domain size (Fig. 4e), which is harmful to exciton dissociation and charge transport.[35] A similar trend is also observed in the 3D images (Fig. S11d–f†).

Grazing incidence wide-angle X-ray scattering (GIWAXS) measurements were performed to evaluate the crystallinity and orientation of the pure material and the active layer. Two-dimensional GIWAXS patterns and the in-plane (IP) and out-of-plane (OOP) line cuts are shown in Fig. 4b and d, f–g and Fig. S12.† Detailed *d*-spacing values are summarized in Table S7 and S8.† The pure BTC film exhibits a strong (100) scattering peak at 0.27 Å^{-1} in the in-plane (IP) direction and weak (010) peaks at 0.57 Å^{-1}, 0.84 Å^{-1} and 1.71 Å^{-1} in the out-of-plane (OOP) direction, indicating a local face-on molecular orientation and overall disordered orientation in the pure films (Fig. S12†).[55] The PM6 : Y6 blend film shows a strong (010) diffraction peak at 1.75 Å^{-1} in the OOP direction and a (100) diffraction peak at 0.29 Å^{-1} in the IP direction, which suggests

Table 2 Summary of contact angles and interaction parameters for PM6, Y6 and BTC

Material	Water contact angle [°]	EG contact angle [°]	γ^d[mN m^{-1}]	γ^p[mN m^{-1}]	Surface tension [mN m^{-1}]	$\chi_{PM6:X}$	$\chi_{BTC:X}$
PM6	105.31	78.01	24.83	0.24	25.08		0.16 K
BTC	97.87	75.09	18.82	2.44	21.27	0.16 K	
Y6	94.58	60.67	36.48	0.55	37.03	1.16 K	2.17 K

that the PM6 : Y6 blend film prefers a face-on molecular orientation.[11] With 15 wt% BTC added to PM6 : Y6, the ternary film demonstrates a stronger (010) diffraction peak at 1.70 $Å^{-1}$ in the OOP direction and a (100) diffraction peak at 0.29 $Å^{-1}$ in the IP direction, indicating an enhanced degree of crystallinity.[47] Moreover, the crystal coherence lengths (CCL) of the ternary film are 24.43 Å for the (010) peak and 59.80 Å for the (100) peak; both are larger than those of the PM6 : Y6 binary film (23.96 Å for the (010) peak and 40.77 Å for the (100) peak).[56] Therefore, the introduction of 15 wt% BTC affords more ordered molecular stacking and orientation, which leads to higher J_{SC}, FF and PCE values in the ternary OSCs. The BTC : Y6 film exhibits weak (010) peaks at 1.75 $Å^{-1}$ in the OOP direction. Consequently, the BTC : Y6 binary OSCs exhibited poor device performance.

Charge transportation, collection, and recombination

We used space-charge-limited current (SCLC) mobility measurements to test the transport ability (details in ESI†). Fig. S13† shows the dark *J*–*V* characteristics of the active layers in hole/electron-only devices. For the PM6 : Y6 blends, the hole (μ_h) and electron (μ_e) mobilities are 5.23×10^{-4} and 4.01×10^{-4} $cm^2\ V^{-1}\ s^{-1}$, respectively, with a μ_h/μ_e ratio of 1.30. When 15 wt% BTC is added to PM6 : Y6, the ternary OSCs exhibit hole (μ_h) and electron (μ_e) mobilities of 6.69×10^{-4} and 5.44×10^{-4} $cm^2\ V^{-1}\ s^{-1}$, respectively, with a μ_h/μ_e ratio of 1.23. These results indicate that the addition of BTC can slightly enhance mobilities and lead to a more balanced μ_h/μ_e ratio in the ternary blend, which favors obtaining a higher FF and J_{SC}.[57,58]

The photoluminescence (PL) spectra of the pure material and the blend films were measured with excitation at 525 nm (Fig. S14†). The BTC and PM6 films show an intense emission peak at 718 nm and a relatively weak emission at 688 nm. The PM6 : BTC blend film with 15 wt% BTC shows a weakened emission originating from PM6 without the emission from BTC, implying that there should be energy transfer between PM6 and BTC.[45] To evaluate charge recombination, the dependence of V_{OC} and J_{SC} on incident light intensity (P_{light}) was performed. Fig. 5b presents plots of the variation of V_{OC} with P_{light} with the linear relationship $V_{OC} = \varepsilon kT\ln(P_{light})/e$ + constant.[59,60] The slopes of the binary and ternary OSCs are 1.07 *kT*/e and 1.03 *kT*/e, respectively, referring to the lower degree of trap-assisted recombination in the ternary blend. The J_{SC} *vs.* light intensity dependence curves ($J_{SC} \propto P_{light}^{\alpha}$) are presented in Fig. 5c, in which the α value indicates a competition between bimolecular recombination and carrier extraction.[61,62] Similar exponential factor α values of 0.965 and 0.966 are calculated for the binary and ternary OSCs, respectively. Both α values are close to 1, suggesting that bimolecular recombination is suppressed in the binary and ternary OSCs.

The photocurrent (J_{ph}) *versus* effective voltage (V_{eff}) measurement was performed to assess the exciton dissociation and charge extraction, and the J_{ph} *versus* V_{eff} plots are presented in Fig. 5d.[63,64] J_{ph} is defined as $J_{ph} = J_{light} - J_{dark}$, in which J_{light} and J_{dark} are the current densities under standard illumination and in the dark, respectively. The charge collection probability $P(E, T)$ value of the ternary OSCs is 0.89, which is slightly higher than the 0.87 of the binary OSCs, and the J_{ph} arrives at the saturated state more rapidly, suggesting more efficient charge extraction and collection in the ternary OSCs, thereby leading to increased J_{SC} and FF.[65]

To test the universality of the BTC molecule, ternary OSCs with a PM6 : L8-BO system were fabricated and analyzed. Binary and ternary OSCs were produced by spin-coating and supplemented with 0.3 vol% 1,8-diiodooctane (DIO). The donor/acceptor weight ratio of the ternary OSCs was 1 : 0.15 : 1.2. The detailed photovoltaic parameters and statistics of the PCE values are presented in Table 1 and Fig. 2d, respectively. The chemical structure of L8-BO and the device parameters are provided in Fig. S15 and S16 and Table S9 and S10.† Owing to the good miscibility of BTC with PM6, the PCE improved from 17.62% for the PM6 : L8-BO binary OSCs to 18.41% for the PM6 : BTC : L8-BO ternary OSCs when incorporating 15 wt% BTC. The *J*–*V* curves and the corresponding EQE curves are shown in Fig. S17.† The J_{SC} values calculated from the EQE spectra of PM6 : L8BO and PM6 : BTC : L8BO are 25.10 and 25.63 mA cm^{-2}, respectively, which is consistent with the *J*–*V* measurement (~5% mismatch). The enhanced PCE was derived from the simultaneous improvement of the V_{OC}, J_{SC} and FF values, indicating the favorable effect of BTC as the third component in the PM6 : L8-BO system.

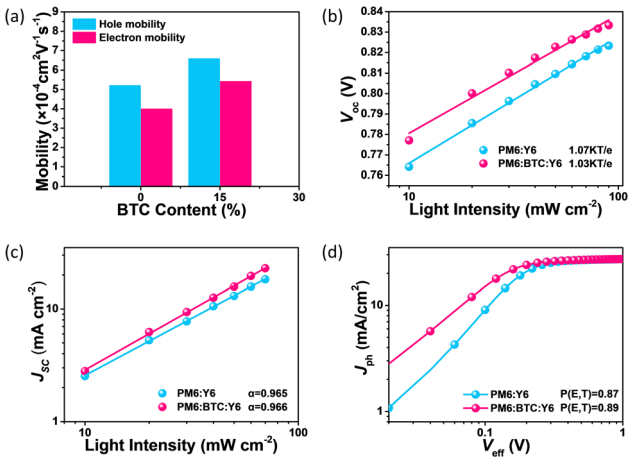

Fig. 5 (a) Statistical mobility values of hole-only and electron-only diodes. Light intensity dependence of the (b) V_{OC} and (c) J_{SC} of the binary and optimized ternary OSCs, and (d) the J_{ph}–V_{eff} plots of the PM6 : Y6 binary and BTC-based ternary OSCs.

Conclusions

In summary, a large-bandgap SM donor, BTC, with *meta*-alkylthio-phenyl-substituted BDT as the core, has been developed to construct high-performance ternary OSCs. Owing to the appropriate energy level, complementary absorption, moderate crystallinity and good compatibility with PM6, the incorporation of 15 wt% BTC into the PM6 : Y6 binary blend leads to enhanced photo harvesting, increased face-on crystallinity, higher and balanced charge mobilities, and reduced charge recombination. Therefore, the ternary OSCs exhibit a PCE of

17.32% with synchronously improved V_{OC}, J_{SC} and FF. Furthermore, a PCE enhancement from 17.62% to 18.41% was achieved when L8-BO was utilized as the acceptor material, indicating the universality of the BTC molecule as the third component in constructing high-performance ternary OSCs. This work provides a novel small-molecule donor and promising molecular design to finely tune the absorption spectra, molecular packing and energy levels of SM donors to construct high-performance ternary OSCs.

Conflicts of interest

There are no conflicts to declare.

Acknowledgements

We are grateful to the financial support from NSF of China (62104197; 62004129). G. L would like to acknowledge the financial support from Shenzhen Science and Technology Innovation Commission (Project No. JCYJ20200109105003940); Research Grants Council of Hong Kong (GRF grant 15221320, CRF C5037-18G, C7018-20G); and the Hong Kong Polytechnic University funds (Sir Sze-yuen Chung Endowed Professorship Fund (8-8480), and RISE (Q-CDA5)).

Notes and references

1 W. Huang, Z. Jiang, K. Fukuda, X. Jiao, C. R. McNeill, T. Yokota and T. Someya, *Joule*, 2020, **4**, 128–141.
2 Z. Chen, W. Song, K. Yu, J. Ge, J. Zhang, L. Xie, R. Peng and Z. Ge, *Joule*, 2021, **5**, 2395–2407.
3 V. V. Brus, J. Lee, B. R. Luginbuhl, S. Ko, G. C. Bazan and T. Nguyen, *Adv. Mater.*, 2019, **31**, 1900904.
4 J. Jing, S. Dong, K. Zhang, Z. Zhou, Q. Xue, Y. Song, Z. Du, M. Ren and F. Huang, *Adv. Energy Mater.*, 2022, 2200453.
5 X. Huang, L. Zhang, Y. Cheng, J. Oh, C. Li, B. Huang, L. Zhao, J. Deng, Y. Zhang, Z. Liu, F. Wu, X. Hu, C. Yang, L. Chen and Y. Chen, *Adv. Funct. Mater.*, 2022, **32**, 2108634.
6 Z. Hu, J. Wang, X. Ma, J. Gao, C. Xu, K. Yang, Z. Wang, J. Zhang and F. Zhang, *Nano Energy*, 2020, **78**, 105376.
7 Y. Lin, J. Wang, Z.-G. Zhang, H. Bai, Y. Li, D. Zhu and X. Zhan, *Adv. Mater.*, 2015, **27**, 1170–1174.
8 W. Zhao, S. Li, H. Yao, S. Zhang, Y. Zhang, B. Yang and J. Hou, *J. Am. Chem. Soc.*, 2017, **139**, 7148–7151.
9 S. Holliday, R. S. Ashraf, A. Wadsworth, D. Baran, S. A. Yousaf, C. B. Nielsen, C.-H. Tan, S. D. Dimitrov, Z. Shang, N. Gasparini, M. Alamoudi, F. Laquai, C. J. Brabec, A. Salleo, J. R. Durrant and I. McCulloch, *Nat. Commun.*, 2016, **7**, 11585.
10 Z.-P. Yu, Z.-X. Liu, F.-X. Chen, R. Qin, T.-K. Lau, J.-L. Yin, X. Kong, X. Lu, M. Shi, C.-Z. Li and H. Chen, *Nat. Commun.*, 2019, **10**, 2152.
11 J. Yuan, Y. Zhang, L. Zhou, G. Zhang, H.-L. Yip, T.-K. Lau, X. Lu, C. Zhu, H. Peng, P. A. Johnson, M. Leclerc, Y. Cao, J. Ulanski, Y. Li and Y. Zou, *Joule*, 2019, **3**, 1140–1151.
12 C. Li, J. Zhou, J. Song, J. Xu, H. Zhang, X. Zhang, J. Guo, L. Zhu, D. Wei, G. Han, J. Min, Y. Zhang, Z. Xie, Y. Yi, H. Yan, F. Gao, F. Liu and Y. Sun, *Nat. Energy*, 2021, **6**, 605–613.
13 Y. Cui, H. Yao, J. Zhang, K. Xian, T. Zhang, L. Hong, Y. Wang, Y. Xu, K. Ma, C. An, C. He, Z. Wei, F. Gao and J. Hou, *Adv. Mater.*, 2020, **32**, 1908205.
14 R. Ma, T. Liu, Z. Luo, Q. Guo, Y. Xiao, Y. Chen, X. Li, S. Luo, X. Lu, M. Zhang, Y. Li and H. Yan, *Sci. China: Chem.*, 2020, **63**, 325–330.
15 L. Wang, C. Guo, X. Zhang, S. Cheng, D. Li, J. Cai, C. Chen, Y. Fu, J. Zhou, H. Qin, D. Liu and T. Wang, *Chem. Mater.*, 2021, **33**, 8854–8862.
16 M. Guan, W. Tao, L. Xu, Y. Qin, J. Zhang, S. Tan, M. Huang and B. Zhao, *J. Mater. Chem. A*, 2022, **10**, 9746–9752.
17 Q. An, F. Zhang, J. Zhang, W. Tang, Z. Deng and B. Hu, *Energy Environ. Sci.*, 2016, **9**, 281–322.
18 J. Wang, C. Han, F. Bi, D. Huang, Y. Wu, Y. Li, S. Wen, L. Han, C. Yang, X. Bao and J. Chu, *Energy Environ. Sci.*, 2021, **14**, 5968–5978.
19 C. Zhu, J. Yuan, F. Cai, L. Meng, H. Zhang, H. Chen, J. Li, B. Qiu, H. Peng, S. Chen, Y. Hu, C. Yang, F. Gao, Y. Zou and Y. Li, *Energy Environ. Sci.*, 2020, **13**, 2459–2466.
20 L. Zhan, S. Li, T.-K. Lau, Y. Cui, X. Lu, M. Shi, C.-Z. Li, H. Li, J. Hou and H. Chen, *Energy Environ. Sci.*, 2020, **13**, 635–645.
21 T. Liu, R. Ma, Z. Luo, Y. Guo, G. Zhang, Y. Xiao, T. Yang, Y. Chen, G. Li, Y. Yi, X. Lu, H. Yan and B. Tang, *Energy Environ. Sci.*, 2020, **13**, 2115–2123.
22 H. Xia, Y. Zhang, W. Deng, K. Liu, X. Xia, C. Su, U. Jeng, M. Zhang, J. Huang, J. Huang, C. Yan, W. Wong, X. Lu, W. Zhu and G. Li, *Adv. Mater.*, 2022, **34**, 2107659.
23 Y. Chang, J. Zhang, Y. Chen, G. Chai, X. Xu, L. Yu, R. Ma, H. Yu, T. Liu, P. Liu, Q. Peng and H. Yan, *Adv. Energy Mater.*, 2021, **11**, 2100079.
24 V. Gupta, V. Bharti, M. Kumar, S. Chand and A. J. Heeger, *Adv. Mater.*, 2015, **27**, 4398–4404.
25 L. Lu, W. Chen, T. Xu and L. Yu, *Nat. Commun.*, 2015, **6**, 7327.
26 P. Cheng, R. Wang, J. Zhu, W. Huang, S. Chang, L. Meng, P. Sun, H. Cheng, M. Qin, C. Zhu, X. Zhan and Y. Yang, *Adv. Mater.*, 2018, **30**, 1705243.
27 X. Ma, W. Gao, J. Yu, Q. An, M. Zhang, Z. Hu, J. Wang, W. Tang, C. Yang and F. Zhang, *Energy Environ. Sci.*, 2018, **11**, 2134–2141.
28 H. Jiang, X. Li, J. Wang, S. Qiao, Y. Zhang, N. Zheng, W. Chen, Y. Li and R. Yang, *Adv. Funct. Mater.*, 2019, **29**, 1903596.
29 Z. Hu, J. Wang, Z. Wang, W. Gao, Q. An, M. Zhang, X. Ma, J. Wang, J. Miao, C. Yang and F. Zhang, *Nano Energy*, 2019, **55**, 424–432.
30 R. Sun, W. Wang, H. Yu, Z. Chen, X. Xia, H. Shen, J. Guo, M. Shi, Y. Zheng, Y. Wu, W. Yang, T. Wang, Q. Wu, Y. Michael Yang, X. Lu, J. Xia, C. J. Brabec, H. Yan, Y. Li and J. Min, *Joule*, 2021, **5**, 1548–1565.
31 W. Song, Y. Liu, B. Fanady, Y. Han, L. Xie, Z. Chen, K. Yu, X. Peng, X. Zhang and Z. Ge, *Nano Energy*, 2021, **86**, 106044.
32 G. Liu, R. Xia, Q. Huang, K. Zhang, Z. Hu, T. Jia, X. Liu, H. Yip and F. Huang, *Adv. Funct. Mater.*, 2021, **31**, 2103283.
33 K.-N. Zhang, Z.-N. Jiang, T. Wang, J.-W. Qiao, L. Feng, C.-C. Qin, H. Yin, S.-K. So and X.-T. Hao, *Nano Energy*, 2021, **79**, 105513.

34 Q. An, J. Wang, X. Ma, J. Gao, Z. Hu, B. Liu, H. Sun, X. Guo, X. Zhang and F. Zhang, *Energy Environ. Sci.*, 2020, **13**, 5039–5047.
35 W. Xu, X. Ma, J. H. Son, S. Y. Jeong, L. Niu, C. Xu, S. Zhang, Z. Zhou, J. Gao, H. Y. Woo, J. Zhang, J. Wang and F. Zhang, *Small*, 2022, **18**, 2104215.
36 J. Song, C. Li, L. Zhu, J. Guo, J. Xu, X. Zhang, K. Weng, K. Zhang, J. Min, X. Hao, Y. Zhang, F. Liu and Y. Sun, *Adv. Mater.*, 2019, **31**, 1905645.
37 K. Li, Y. Wu, Y. Tang, M. Pan, W. Ma, H. Fu, C. Zhan and J. Yao, *Adv. Energy Mater.*, 2019, **9**, 1901728.
38 J. Gao, J. Wang, Q. An, X. Ma, Z. Hu, C. Xu, X. Zhang and F. Zhang, *Sci. China: Chem.*, 2020, **63**, 83–91.
39 M.-A. Pan, T.-K. Lau, Y. Tang, Y.-C. Wu, T. Liu, K. Li, M.-C. Chen, X. Lu, W. Ma and C. Zhan, *J. Mater. Chem. A*, 2019, **7**, 20713–20722.
40 X. Li, M.-A. Pan, T.-K. Lau, W. Liu, K. Li, N. Yao, F. Shen, S. Huo, F. Zhang, Y. Wu, X. Li, X. Lu, H. Yan and C. Zhan, *Chem. Mater.*, 2020, **32**, 5182–5191.
41 Q. Ma, Z. Jia, L. Meng, J. Zhang, H. Zhang, W. Huang, J. Yuan, F. Gao, Y. Wan, Z. Zhang and Y. Li, *Nano Energy*, 2020, **78**, 105272.
42 L. Zhan, S. Li, X. Xia, Y. Li, X. Lu, L. Zuo, M. Shi and H. Chen, *Adv. Mater.*, 2021, **33**, 2007231.
43 D. Su, M.-A. Pan, Z. Liu, T.-K. Lau, X. Li, F. Shen, S. Huo, X. Lu, A. Xu, H. Yan and C. Zhan, *Chem. Mater.*, 2019, **31**, 8908–8917.
44 X. Ma, A. Zeng, J. Gao, Z. Hu, C. Xu, J. H. Son, S. Y. Jeong, C. Zhang, M. Li, K. Wang, H. Yan, Z. Ma, Y. Wang, H. Y. Woo and F. Zhang, *Natl. Sci. Rev.*, 2021, **8**, nwaa305.
45 T. Yan, J. Ge, T. Lei, W. Zhang, W. Song, B. Fanady, D. Zhang, S. Chen, R. Peng and Z. Ge, *J. Mater. Chem. A*, 2019, **7**, 25894–25899.
46 X. Chen, Q. Zhang, D. Wang, X. Xu, Z. Wang, Y. Li, H. Zhu, X. Lu, W. Chen, H. Qiu and C.-Z. Li, *Sol. RRL*, 2020, **4**, 2000537.
47 L. Xu, W. Tao, H. Liu, J. Ning, M. Huang, B. Zhao, X. Lu and S. Tan, *J. Mater. Chem. A*, 2021, **9**, 11734–11740.
48 J. Qin, C. An, J. Zhang, K. Ma, Y. Yang, T. Zhang, S. Li, K. Xian, Y. Cui, Y. Tang, W. Ma, H. Yao, S. Zhang, B. Xu, C. He and J. Hou, *Sci. China Mater.*, 2020, **63**, 1142–1150.
49 M. Bilal Ahmed Siddique, R. Hussain, S. Ali Siddique, M. Yasir Mehboob, Z. Irshad, J. Iqbal and M. Adnan, *ChemistrySelect*, 2020, **5**, 7358–7369.
50 Y. Zhang and G. Li, *Acc. Mater. Res.*, 2020, **1**, 158–171.
51 Q. An, J. Wang, W. Gao, X. Ma, Z. Hu, J. Gao, C. Xu, M. Hao, X. Zhang, C. Yang and F. Zhang, *Sci. Bull.*, 2020, **65**, 538–545.
52 L. Chang, M. Sheng, L. Duan and A. Uddin, *Org. Electron.*, 2021, **90**, 106063.
53 W. Xu, X. Zhu, X. Ma, H. Zhou, X. Li, S. Y. Jeong, H. Y. Woo, Z. Zhou, Q. Sun and F. Zhang, *J. Mater. Chem. A*, 2022, **10**, 13492–13499.
54 J. Zhang, Y. Li, Z. Peng, F. Bai, L.-K. Ma, H. Ade, Z. Li and H. Yan, *Mater. Chem. Front.*, 2020, **4**, 1729–1738.
55 P. Müller-Buschbaum, *Adv. Mater.*, 2014, **26**, 7692–7709.
56 J. Lv, Y. Feng, J. Fu, J. Gao, R. Singh, M. Kumar, M. Kim, H. Tang, S. Lu, W. Zhang, I. McCulloch, J. Li and Z. Kan, *Sol. RRL*, 2020, **4**, 1900403.
57 T. Xu, J. Lv, K. Yang, Y. He, Q. Yang, H. Chen, Q. Chen, Z. Liao, Z. Kan, T. Duan, K. Sun, J. Ouyang and S. Lu, *Energy Environ. Sci.*, 2021, **14**, 5366–5376.
58 Y. Ma, D. Cai, S. Wan, P. Yin, P. Wang, W. Lin and Q. Zheng, *Natl. Sci. Rev.*, 2020, **7**, 1886–1895.
59 X. Wang, Z. Du, K. Dou, H. Jiang, C. Gao, L. Han and R. Yang, *Adv. Energy Mater.*, 2019, **9**, 1802530.
60 X. Ma, Q. An, O. A. Ibraikulov, P. Lévêque, T. Heiser, N. Leclerc, X. Zhang and F. Zhang, *J. Mater. Chem. A*, 2020, **8**, 1265–1272.
61 Z. Hu, F. Zhang, Q. An, M. Zhang, X. Ma, J. Wang, J. Zhang and J. Wang, *ACS Energy Lett.*, 2018, **3**, 555–561.
62 Y. Lin, Y. Firdaus, M. I. Nugraha, F. Liu, S. Karuthedath, A. Emwas, W. Zhang, A. Seitkhan, M. Neophytou, H. Faber, E. Yengel, I. McCulloch, L. Tsetseris, F. Laquai and T. D. Anthopoulos, *Adv. Sci.*, 2020, **7**, 1903419.
63 Q. An, F. Zhang, W. Gao, Q. Sun, M. Zhang, C. Yang and J. Zhang, *Nano Energy*, 2018, **45**, 177–183.
64 Y. Ma, D. Cai, S. Wan, P. Wang, J. Wang and Q. Zheng, *Angew. Chem., Int. Ed.*, 2020, **59**, 21627–21633.
65 X. Liu, R. Ma, Y. Wang, S. Du, J. Tong, X. Shi, J. Li, X. Bao, Y. Xia, T. Liu and H. Yan, *ACS Appl. Mater. Interfaces*, 2021, **13**, 11117–11124.

